AIAA JOURNAL
Vol. 47, No. 1, January 2009

# Improvement of Axial Load Capacity of Elliptical Cylindrical Shells

Maurizio Paschero* and Michael W. Hyer†
*Virginia Polytechnic Institute and State University, Blacksburg, Virginia, 24061*

DOI: 10.2514/1.37012

**By varying the thickness of the cylinder wall with circumferential position, the axial buckling capacities of homogeneous, isotropic cylindrical shells with elliptical cross sections are improved. The classic buckling stress relation for a uniform-thickness homogeneous, isotropic circular cylindrical shell is applied to cylinders with elliptical cross sections. It is assumed that this relation can be used to design the wall thicknesses of elliptical cylinders as a function of circumferential location to compensate for the negative effects of the variation of the radius of curvature with circumferential location. Three variable-thickness elliptical cylinder designs are proposed, and analytical expressions for the thickness variation, cross-sectional area, axial buckling stress, axial buckling stress resultant, and axial buckling load for each design are derived. Predictions from the analytical development are then compared with finite element analyses of the three designs. So-called small and large cylinders with three values of eccentricity are considered. The comparisons between the finite element results and the analytic predictions are quite good. It is shown that considerable improvement in axial buckling capacity can be achieved with the thickness-tailoring technique, and in some cases the axial capacity of the circular cylinder with the same circumference is achieved.**

## Nomenclature

$a$ = major radius, m
$b$ = minor radius, m
$E$ = Young's modulus, Pa
$\mathcal{E}$ = normalized complete elliptical integral of second kind
$e$ = eccentricity
$h$ = wall thickness, m
$N$ = axial stress resultant, N/m
$P$ = axial load, N
$R$ = radius of curvature, m
$s$ = arc length, m
$\nu$ = Poisson's ratio
$\sigma$ = axial stress, Pa
$\bar{\sigma}$ = average axial stress, Pa

## I. Introduction and Background

CYLINDRICAL structures are effective in resisting a variety of loads, including axial compression, torsion, internal pressure, overall bending, and combinations of these. In particular, cylindrical structures with circular cross sections have been used in a variety of aerospace applications. Even though a circular cross section may be the most effective structural shape, in certain applications a noncircular cross section may have advantages. Blended wing–fuselage aircraft designs could benefit by using a noncircular fuselage. Geometric constraints may dictate that fuel tanks for other aerospace applications be noncircular. Kempner and Chen [1] concluded that oval cylinders with moderate-to-large eccentricities would be not very sensitive to initial imperfections. Hutchinson [2] reached similar conclusions for noncircular cylinders. However, in many applications a noncircular geometry leads to reduced structural performance. Specifically, the axial stress level to cause buckling of a geometrically perfect, homogeneous, isotropic circular cylindrical shell subjected to an axial load can be estimated through the classical equation [3,4]

$$(\sigma_{cr})_{circle} = \frac{Eh}{R\sqrt{3(1-\nu^2)}} \tag{1}$$

where the subscript cr denotes critical. The axial buckling stress in Eq. (1) is assumed to be uniform through the thickness of the wall. For a cylindrical shell with a smooth and convex noncircular cross section obtained, for example, by deforming the original circular cross section into an elliptical cross section with the same circumference, the radius of curvature varies with circumferential location. However, Eq. (1) can be used to estimate the axial buckling stress if the maximum radius of curvature of the cross section is substituted for $R$ in Eq. (1) [5]:

$$(\sigma_{cr})_{ellipse} = \frac{Eh}{R_{max}\sqrt{3(1-\nu^2)}} \tag{2}$$

Because $R_{max}$ for the noncircular cylinder is greater than $R$ for the original circular cylinder, the buckling stress, and therefore the buckling load, of the noncircular cylinder is less than that of the circular cylinder. Specifically, as will be shown in Sec. IV, for a cylinder with an elliptical cross section with an eccentricity of 0.70 (which results in a ratio of the minor radius to the major radius of about 0.70), the axial buckling stress is estimated to be approximately 40% less than the original circular cylinder. The prebuckling deformations of the original circular cylinder and an elliptical cylinder with the same circumference, an eccentricity of 0.70, and both with S1 simply supported boundary conditions [6] at (or slightly less than) the buckling load level, as predicted by geometrically nonlinear finite element analyses, are illustrated in Figs. 1a and 1b, respectively. As seen, the more relevant deformations for both cases are confined to the ends of the cylinders, forming boundary layers, a characteristic typical of cylindrical structures. The width of the boundary layer depends on the radius of curvature of the cylinder and an expression for the boundary layer length as a function of the radius of curvature can be derived [7]. More important, however, the deformations of the circular cylinder involve all circumferential locations (and are axisymmetric, as they should be), whereas those of the elliptical

Received 5 February 2008; revision received 24 June 2008; accepted for publication 18 July 2008. 

*Postdoctoral, INFO-COM Department; currently University of Rome La Sapienza, Via Eudossiana, 18, 00184 Roma, Italy.
†N. Waldo Harrison Professor, Department of Engineering Science and Mechanics; hyerm@vt.edu. Fellow AIAA.

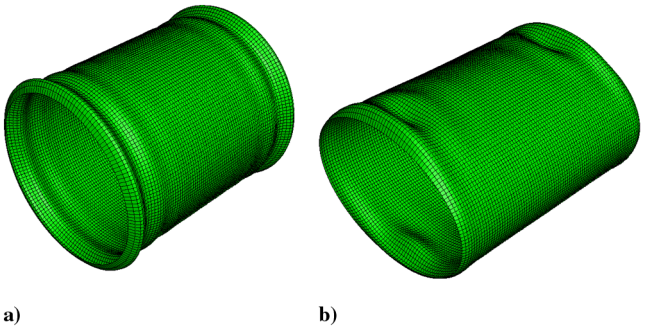

a) b)

**Fig. 1 Prebuckling deformed shape of axially loaded simply supported cylindrical shells: a) circular cross section and b) elliptical cross section.**

cylinder are confined to flatter regions of the cross sections where the radius of curvature is the greatest. The deformation behavior of the elliptical cylinder suggests that material in the cylinder wall is not being used as effectively as it could to resist cylinder buckling. The flatter portions of the elliptical cross section are critically stressed, whereas the more highly curved sides are understressed. Of course here the term under-stressed is in relation to the stress necessary to cause local buckling. It would seem that if all of the material in the cross section were critically stressed, the axial buckling load of the elliptical cylinder would increase. Ideally, the buckling load of the elliptical cylinder could be restored to the value for the original circular cylinder.

To expand upon this concept, based on Eq. (1), for a given isotropic material (i.e., for given values of $E$ and $\nu$) the stress to cause buckling is dependent only on the ratio of the wall thickness to the radius $h/R$. In fact, the buckling stress is directly proportional to the minimum value of this ratio, which for a noncircular cylinder with a uniform wall thickness is a minimum where the radius of curvature is a maximum. Because, for an elliptical cylinder, continuing with this particular noncircular cross section as an example, the variation of the radius of curvature with circumferential position is known from the geometry of the ellipse, perhaps the thickness of the cylinder wall could be varied with circumferential position so as to keep the ratio of the wall thickness to the radius constant with circumferential position and have no circumferential location where the ratio is a minimum. Based on Eq. (1), for a given material the thickness of the cylinder wall is the only parameter that can be varied in an effort to offset the loss of axial buckling load due to the noncircular cross-sectional geometry. The objective of this paper is to design the variation of wall thickness of an elliptical cylinder with circumferential position so as to mitigate the loss of buckling capacity relative to the original circular cylinder. Strictly speaking, for the case of the wall thickness and the radius of curvature varying as a function of circumferential position, the stresses within the cylinder could become more complex than for a uniform-thickness circular cylinder. Therefore, to keep the concept simple, the designs developed will be based solely on the use of Eq. (1). However, Eq. (1) is based on a derivation employing numerous simplifying assumptions (e.g., a membrane prebuckling state). Thus, to confirm or refute any predicted gains in buckling performance using the classical buckling equation shown in Eq. (1) for design purposes, finite element calculations considering a geometrically nonlinear prebuckling state will also be presented and discussed for variable wall-thickness cylinders designed using Eq. (1).

The next section of the paper presents a brief overview of some of the past work on the stability of noncircular cylinders. Then, in the following section following, the development of variable-thickness noncircular cylinders based on Eq. (1) will be presented. Only elliptical, noncircular cross sections will be considered, mainly because of the convenience of the algebra of such cross sections. However, the concepts developed can be generalized to other noncircular cross sections. It should be noted that material tailoring of elliptical fiber-reinforced composite cylinders has been discussed in [8] as a contrast to the thickness-tailoring concept being discussed herein.

## II. Review of Related Past Work

The vast majority of the investigations of the stability of cylinders has focused on circular cylinders. However, as early as 1935 Lundquist and Burke [9] studied the torsional stability of elliptical cylinders. A short time later Heck [10] considered elliptical cylinders in pure bending. In 1951 Marguerre [11] proposed expressing the curvature of an elliptical cross section by using the trigonometric series

$$\frac{1}{R(s)} = \frac{1}{R_0}\left(1 + \sum_{k=1}^{\infty} a_k \cos\left(\frac{4k\pi s}{C}\right)\right) \tag{3}$$

where $R_o$ is the average radius, $s$ the circumferential arc length coordinate, and $C$ the circumference. This expression can actually be used for any noncircular section having two perpendicular axes of symmetry. Another interpretation of Eq. (3) is to consider a noncircular cross section as a perturbation of one that is circular.

Kempner and Chen [5,12] used Marguerre's expression and a variational approach to develop a geometrically nonlinear analysis of an oval cylinder subjected to an axial load. They considered an infinitely long cylinder and modeled the variable curvature with a two-term series using Eq. (3). Numerical results were derived through the Ritz method. The main results of their work can be summarized by saying that the buckling phenomenon for a noncircular shell starts in the region having minimum curvature, in other words the location where the shell is flatter, as was illustrated for the prebuckling deformations in Fig. 1b. This result can also be expressed by saying that the buckling load of a thin shell having a noncircular section approaches the buckling load of a circular section having radius equal to the maximum radius of curvature of the noncircular cross section. This characteristic was discussed in relation to Eq. (2), and a direct consequence of this behavior is that the more the eccentricity of a section increases, the more the buckling load decreases relative to the original circular cylinder. Another interesting result found by Kempner and Chen is that although the buckling load of a noncircular cylindrical shell decreases relative to the original circular cylinder, the postbuckling stiffness of an oval section is larger than the postbuckling stiffness of a circular section. This increased stiffness is due to the fact that the high curvature regions of the cross section at the ends of the major radius do not participate in the postbuckling buckling deformations and thus are able to continue to support a load. Further theoretical studies on the postbuckling of noncircular cylindrical shells [1,2] highlight that the more the eccentricity of the section increases, the more the postbuckling snap-though phenomenon, which occurs when the axial load exceeds the buckling value, is moderated. Experimental results were found to be in good agreement with the theoretical predictions. More accurate analyses, including more nonlinear terms in the strain-displacement relations, were performed in [13], where the buckling behaviors of axially compressed elliptical cones and cylinders, for both the perfect and imperfect cases, were studied. In [14] the effect of the introduction of clamped boundary conditions on the stability of isotropic noncircular cylinders was studied in order to account for nonmembrane prebuckling deformations. The correction due to the effects of the clamped boundaries on the buckling load predicted by theories based on infinite-length cylinders was found to be moderate for low eccentricity sections. Theoretical predictions were confirmed by experimental results [15].

Though the current paper considers only isotropic materials, it is of interest to note a few of the studies of noncircular composite cylinders. These studies are more recent than the studies of isotropic shells. An early contribution in this direction is found in [16], where the instability under axial compression of oval symmetric and antisymmetric cross-ply laminated cylinders was studied. Sun [17] showed that for a wide range of eccentricities the stability performance of symmetric cross-ply noncircular infinite-length cylinders is quite insensitive to imperfections. An analysis taking into account the most general boundary conditions was performed in [18,19] using a Galerkin approach based on a Marguerre-like series expansion of the radius of curvature. In this work it was shown that

the coupling between axial and circumferential modes becomes more relevant as the eccentricity increases. It was also shown that noncircular laminated composite shells are less sensitive to imperfections compared with the equivalent circular case. This behavior becomes more evident as the eccentricity increases. In [20,21] a Love-type parabolic through-thickness shear deformation shell theory was applied to a noncircular laminated shell. The buckling load of a cross-ply laminated noncircular cylinder under axial compression was derived through the Galerkin method. The results of this work showed that taking into account shear deformations produces a more conservative estimation of the axial buckling load. It was also observed that the effect of transverse shear deformations decreases as the eccentricity increases. In more recent years a formulation taking into account transverse normal and transverse shear deformations was proposed [22,23]. In this work trigonometric series expansions of the displacements, including higher-order terms, were assumed. Generalized variables associated with zigzag functions were included in the model. The solutions obtained through a finite element approach showed that the coupling between axial and circumferential modes increases as the eccentricity increases, as was found in [18,19]. As mentioned, recently Sun and Hyer [8] investigated the effects of the fiber orientation on the stability of elliptical $[\pm\theta/0/90]_S$ composite cylinders. A procedure to vary the angle $\theta$ around the circumference to improve axial load capacity relative to the case of $\theta = 45$ deg all around the circumference (a quasi-isotropic elliptical cylinder) was proposed and numerically validated. An improvement of the axial load capability up to 30% was obtained with no prebuckling material failure and little increase in postbuckling material failure. Considering a torsional loading, Haynie and Hyer [24] recently considered buckling, postbuckling, and material failure of elliptical composite cylinders with a quasi-isotropic lamination sequence. For the cylinders studied they demonstrated that initial material failure occurred at isolated circumferential locations that were controlled by the local radius of curvature of the elliptical cross section, as opposed to the situation with circular cylinders, where initial failure occurred uniformly around the circumference.

## III. Basis for the Design of Variable-Thickness Elliptical Cylindrical Shells

To continue to expand upon the fact that the axial buckling stress in Eq. (1) depends on the ratio $h/R$, in the present study it will be assumed that the buckling stress of a homogeneous, isotropic cylindrical shell having a cross section with both a circumferentially varying radius of curvature and a circumferentially varying wall thickness is given by

$$\sigma_{\text{cr}} \propto \min_{\text{all around the circumference}} \left\{ \frac{h}{R} \right\} \tag{4}$$

To circumvent there being any location around the circumference of a noncircular cylinder where there is indeed a minimum, it will be further assumed that a variable-thickness homogeneous, isotropic noncircular cylindrical shell can be designed with the condition

$$\frac{h}{R} = \text{const} \qquad \text{all around the circumference} \tag{5}$$

It would seem that the fulfillment of Eq. (5) should guarantee that the cylinder does not have a weaker (in the sense of local buckling) circumferential location that compromises the performance of the entire cylinder. Consequently, the entire elliptical cylinder should be involved in the deformation, thereby increasing the axial load performance of the structure. The cross-sectional shapes that result in the entire cylinder participating in the loss of stability are referred to as shapes of uniform stability and are discussed briefly in a book by Gajewski and Zyczkowski [25]. Here the choice of the constant in Eq. (5) will be addressed in different ways, depending on the details of the specific objective to be achieved. In the following section, three different designs of a variable-thickness elliptical cylindrical shell based on three different choices of the constant in Eq. (5) to meet three specific objectives will be proposed.

## IV. Three Variable-Thickness Elliptical Cylindrical Shell Designs

Consider a uniform-thickness circular cylindrical shell with radius $R_c$, thickness $h_c$, and length $L_c$. Suppose the given circular cross section is made elliptical by assigning to it an eccentricity $e_0$, but the circumference is kept the same as the original circular cylinder, namely $2\pi R_c$. An elliptical cross section can be described parametrically using the parameter $t$ by the radius vector $\mathbf{v}(t)$ defined by

$$\mathbf{v}(t) = (a\cos(t), b\sin(t)) \qquad t \in [0, 2\pi) \tag{6}$$

where, as illustrated in Fig. 2 $a$ and $b$ are the major and the minor radii of the cross section of the midsurface and, as shown, $\mathbf{n}(t)$, $R(t)$, and $h(t)$ are the unit normal, the radius of curvature, and the thickness of the cross section. The arc length in the circumferential direction is measured by the parameter $s$. The eccentricity of an ellipse $e$ is defined as

$$e = \sqrt{1 - \frac{b^2}{a^2}} \tag{7}$$

It should be noted that $e = 0$ when $a = b$, with the ellipse degenerating to a circle. Similarly, $e = 1$ when $b = 0$, with the ellipse degenerating to a flat panel. Based on these arguments it should be clear that in order to have an ellipse the following relation must be fulfilled: $0 \le e < 1$. All the expressions involving the eccentricity derived in the following are meaningful only for this range of values. Using the parametrization of Eq. (6) the unit normal and the radius of curvature can be expressed as

$$\mathbf{n}(t) = \left( \frac{b\cos(t)}{\sqrt{a^2\sin^2(t) + b^2\cos^2(t)}}, \frac{a\sin(t)}{\sqrt{a^2\sin^2(t) + b^2\cos^2(t)}} \right) \tag{8}$$

$t \in [0, 2\pi)$

$$R(t) = \frac{(b^2\cos^2(t) + a^2\sin^2(t))^{\frac{3}{2}}}{ab} \qquad t \in [0, 2\pi) \tag{9}$$

Analytical expressions for radius vectors to the outer and the inner surfaces of the variable-thickness ellipse can be obtained by adding and subtracting, respectively, the quantity $h(t)/2$ along the direction normal to the midsurface, as shown in Fig. 2. The radius vectors describing these surfaces can be written as follows:

$$\mathbf{v}_{\text{out}}(t) = \mathbf{v}(t) + \frac{h(t)}{2}\mathbf{n}(t) \qquad \mathbf{v}_{\text{in}}(t) = \mathbf{v}(t) - \frac{h(t)}{2}\mathbf{n}(t) \tag{10}$$

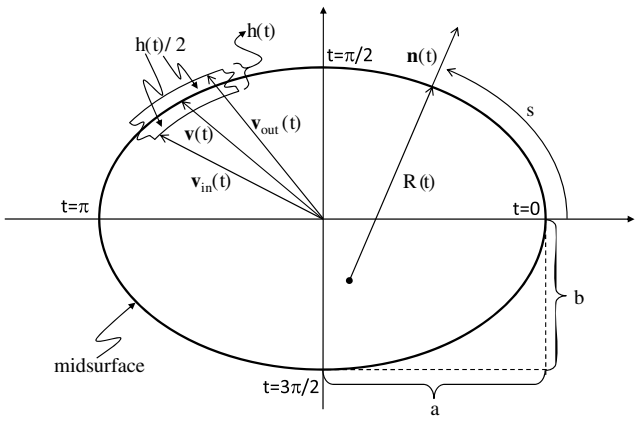


**Fig. 2 Cross section of the midsurface of an elliptical cylinder.**

The major radius $a$ and the minor radius $b$ of an ellipse having an assigned eccentricity $e_0$ and the same circumference as the original circular cylinder are given by

$$a = \frac{R_c}{\mathcal{E}(e_0^2)} \qquad b = \frac{R_c}{\mathcal{E}(e_0^2)}\sqrt{1-e_0^2} \tag{11}$$

where $\mathcal{E}(.)$ is the normalized complete elliptical function of second kind defined by

$$\mathcal{E}(k) = \frac{2}{\pi}\int_0^{\frac{\pi}{2}} \sqrt{1-k\sin^2(\theta)}\,\mathrm{d}\theta \tag{12}$$

It should be noted that when the assigned eccentricity $e_0 = 0$ (i.e., the circular case), Eq. (11) gives correctly $a = R_c$ and $b = R_c$, and when $e_0 = 1$ (i.e., the flat panel case), Eq. (11) gives correctly $a = \pi R_c/2$ and $b = 0$. The minimum and the maximum radii of curvature of an ellipse are related to $a$ and $b$ through the following relations:

$$R_{\min} = \frac{b^2}{a} = \frac{R_c}{\mathcal{E}(e_0^2)}(1-e_0^2) \qquad R_{\max} = \frac{a^2}{b} = \frac{R_c}{\mathcal{E}(e_0^2)}\frac{1}{\sqrt{1-e_0^2}} \tag{13}$$

Based on Eqs. (1), (2), and (13), the ratio between the buckling stress of the constant thickness elliptical (CTE) cylinder, obtained by assigning an eccentricity $e_0$ to the original constant thickness circular (CTC) cylinder, and the original CTC cylinder is predicted to be

$$\frac{\sigma_{\mathrm{CTE}}}{\sigma_{\mathrm{CTC}}} = \frac{R_c}{R_{\max}} = \mathcal{E}(e_0^2)\sqrt{1-e_0^2} \tag{14}$$

It should be noted that the ratio of the buckling stresses between the two cylinders depends only on the assigned eccentricity $e_0$. In Fig. 3 the ratio in Eq. (14) is plotted vs the assigned eccentricity $e_0$. As seen, the buckling stress of a CTE cylinder decreases considerably with increasing eccentricity. For example, about 20% of the stress level is lost when an eccentricity of 0.50 is assigned to the original CTC cylinder. Similarly, about 40% of the stress level is lost for $e_0 = 0.70$ and about 60% for $e_0 = 0.85$. Because the cross-sectional area of the CTC and CTE cylinders are the same, and because the axial stress is uniform through the cylinder wall thickness, the ratio between the buckling load of the CTE cylinder $P_{\mathrm{CTE}}$ and the buckling load of the CTC cylinder $P_{\mathrm{CTC}}$ is also given by Eq. (14).

To make use of the concept of choosing the thickness $h(t)$ of the cross section to be proportional to its radius of curvature $R(t)$ [i.e., Eq. (5)] to counter the decreases illustrated in Fig. 3, the constant in Eq. (5) will be scaled by the ratio between the thickness and the radius of curvature of the original CTC cylinder. Accordingly, the varying thickness of the elliptical cross section $h(t)$ will be assumed to be given by

$$h(t) = \alpha\frac{h_c}{R_c}R(t) \qquad t \in [0, 2\pi) \tag{15}$$

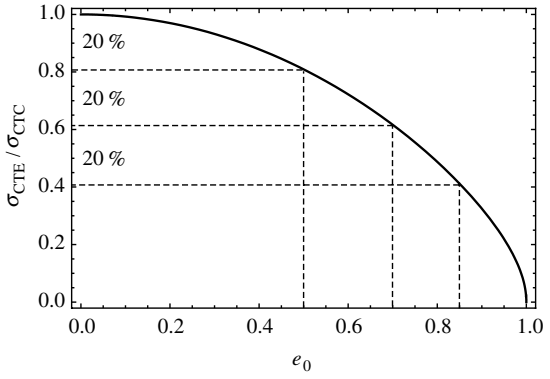


**Fig. 3 Comparison between the buckling stress of elliptical and original circular cylinders.**

where $\alpha$ is a positive scalar quantity. The radius of curvature $R(t)$ of an ellipse having the same circumference as the original circle and an assigned eccentricity $e_0$ can be obtained by substituting Eq. (11) in Eq. (9), that is

$$R(t) = \frac{R_c}{\mathcal{E}(e_0^2)}\sqrt{\frac{(1-e_0^2\cos^2(t))^3}{1-e_0^2}} \qquad t \in [0, 2\pi) \tag{16}$$

Thus, the design of the variable-thickness elliptical (VTE) cylinder (i.e., $h(t)$ vs $t$) is complete once the value of the constant $\alpha$ in Eq. (15) is specified. In the present development, the constant $\alpha$ will be chosen in three different ways, resulting in three different VTE cylinder designs:

1) The buckling stress $\sigma_{\mathrm{VTE}}$ of the VTE cylinder is the same as the buckling stress $\sigma_{\mathrm{CTC}}$ of the original CTC cylinder.

2) The buckling load $P_{\mathrm{VTE}}$ of the VTE cylinder is the same as the buckling load $P_{\mathrm{CTC}}$ of the original CTC cylinder.

3) The cross-sectional area $A_{\mathrm{VTE}}$ of the VTE cylinder is the same as the cross-sectional area $A_{\mathrm{CTC}}$ of the original CTC cylinder.

With the cylinders all the same length, requiring the cross-sectional areas to be identical guarantees that the volume, and consequently the weight, of the VTE cylinder is the same as the weight of the original CTC cylinder. Imposing conditions such as one of the three preceding is necessary because Eq. (5) is simply a statement regarding two geometric variables. The statement does not guarantee that the axial buckling stress in the VTE cylinder is the same as the axial buckling stress in the original CTC cylinder, nor does it guarantee that the cross-sectional area of the variable-thickness wall is the same, or that the axial buckling load, which is directly related to both the axial buckling stress and the cross-sectional area, is the same. Conditions other than Eq. (5) are necessary to guarantee equality, in some sense, of the VTE and the original CTC cylinders.

To specify the three different VTE cylinder designs it is necessary to determine how the three ratios $\sigma_{\mathrm{VTE}}/\sigma_{\mathrm{CTC}}$, $P_{\mathrm{VTE}}/P_{\mathrm{CTC}}$, and $A_{\mathrm{VTE}}/A_{\mathrm{CTC}}$ depend on the selection of the constant $\alpha$. To that end, considering the ratio $\sigma_{\mathrm{VTE}}/\sigma_{\mathrm{CTC}}$ and substituting Eq. (15) in Eq. (4) it can be seen that the buckling stress of a VTE cylinder becomes independent of the circumferential location. That is

$$\sigma_{\mathrm{VTE}} = \beta\frac{h(t)}{R(t)} = \beta\alpha\frac{h_c}{R_c} \tag{17}$$

where $\beta$ is a positive constant of proportionality. Based on Eq. (1), the constant $\beta$ can be defined as

$$\beta = \sigma_{\mathrm{CTC}}\frac{R_c}{h_c} \tag{18}$$

Substituting Eq. (18) in Eq. (17) results in

$$\frac{\sigma_{\mathrm{VTE}}}{\sigma_{\mathrm{CTC}}} = \alpha \tag{19}$$

Considering next the area ratio $A_{\mathrm{VTE}}/A_{\mathrm{CTC}}$, using Eqs. (10) and (15) the area ratio can be analytically evaluated to give

$$\frac{A_{\mathrm{VTE}}}{A_{\mathrm{CTC}}} = \alpha g^2(e_0) \tag{20}$$

where

$$g(e_0) = \frac{1}{\mathcal{E}(e_0^2)}\sqrt{\frac{8-8e_0^2+3e_0^4}{8\sqrt{1-e_0^2}}} \tag{21}$$

Lastly, the ratio $P_{\mathrm{VTE}}/P_{\mathrm{CTC}}$ can be evaluated by simply multiplying Eq. (19) and (20) term by term, using the fact that each of the three designs requires the stress to be constant around the circumference. As a result,

$$\frac{P_{\mathrm{VTE}}}{P_{\mathrm{CTC}}} = \frac{\sigma_{\mathrm{VTE}}}{\sigma_{\mathrm{CTC}}}\frac{A_{\mathrm{VTE}}}{A_{\mathrm{CTC}}} = \alpha^2 g^2(e_0) \tag{22}$$

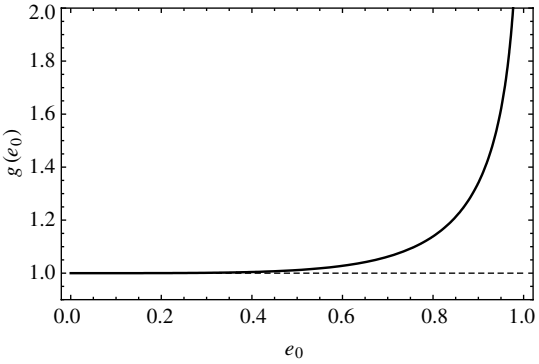


**Fig. 4 Variation of $g(e_0)$ with $e_0$.**

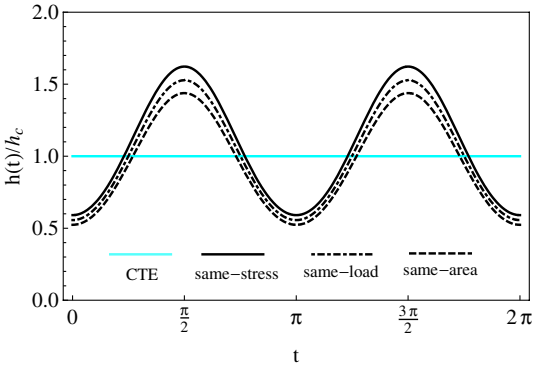


**Fig. 5 Variation of the normalized thickness with the circumferential location for the three designs, $e_0 = 0.7$.**

The relation of Eq. (21) is plotted in Fig. 4. It should be noted that $g(e_0)$ is always greater that one. More precisely, it is very close to the unity when $0 \leq e_0 < 0.6$, then increases very quickly and tends to infinity for $e_0$ approaching one. Now, using Eqs. (19), (20), and (22), the value of the constant $\alpha$ needed to design a VTE cylinder having the same buckling stress, the same buckling load, or the same cross-sectional area (hereafter known simply as same-stress, same-load, and same-area designs) of the original CTC cylinder can be determined. These values of $\alpha$ are listed in Table 1 together with the thickness variation $h(t)$, normalized by the thickness of the original circle $h_c$, for the three designs of interest. These three thickness variations are plotted in Fig. 5 for $e_0 = 0.70$ together with the unit value representing the normalized thickness of the CTE cylinder. From Fig. 5 it should be noted that all the VTE designs allocate a larger thickness to the most flat regions of the ellipse (see Fig. 2, $t = \pi/2$ and $t = 3\pi/2$). Moreover, it can be seen that the thickness profiles associated with the three different VTE designs never intersect each other. This means that for each value of the parameter $t$, the thickness of the same-stress design is larger than the thickness of the same-load design, which, in turn, is larger than the thickness of the same-area design. More precisely, it should be noted that the thickness of the same-load design is exactly the geometric mean between the thickness of the same-stress design and the same-area design.

For the sake of completeness it should be noted that once the radius $R_c$ and the thickness $h_c$ of the original CTC cylinder are given, it is not possible to construct either a CTE cylinder or a VTE cylinder with an assigned eccentricity greater than a critical, or maximum, value without forcing penetration of the inner surfaces of the two opposite sides of the cross section. This critical value of eccentricity is dependent on which of the three particular cylinders is being considered. More precisely, the critical eccentricity for each particular cylinder can be defined by equating the ratio $h_c/R_c$ to a dimensionless function depending only on the assigned eccentricity $e_0$. The value of the eccentricity fulfilling the equality is the maximum eccentricity that can be assigned to the original circular cross section. This value will be referred as critical eccentricity and will be denoted by the symbol $e_{\mathrm{cr}}$. The functions determining the critical eccentricity for each particular cylinder are listed in Table 2 and are plotted in Fig. 6. Examination of Fig. 6 shows that when the ratio $h_c/R_c = 2$ it is impossible to assign any eccentricity to the original circular cylindrical shell for any of the particular cylinders. This geometric constraint can be explained referring to Fig. 2 and realizing that when $h_c/R_c = 2$ the cylindrical shell becomes a solid cylinder of radius $2R_c$. Another relevant point to be noted in Fig. 6 is that when the ratio $h_c/R_c$ approaches zero the critical eccentricity approaches one for all cylinders. This means that if the thickness of the original circular cylinder approaches zero, then it can be deformed until it becomes a flat plate. Based on these arguments, for the original CTC cylinder the following constraint must be fulfilled:

$$0 < \frac{h_c}{R_c} < 2 \tag{23}$$

For most cylindrical shells this condition is not a problem. It should also be noted from Fig. 6 that the relations for the three VTE designs never intersect each other. This happens because the thicknesses of the three VTE cylinders are proportional one to each other, as illustrated in Fig. 5 and Table 1. More precisely, the same-load design relation is bounded by the more restrictive same-stress design and the less restrictive same-area design. This means that if it is possible to construct the same-stress VTE cylinder for a given value of $h_c/R_c$ and an assigned eccentricity $e_0$, then it is possible to construct the same-load and the same-area VTE cylinders for the same assigned eccentricity. It should be finally noted that the relation for the CTE cylinder intersects both the same-load and the same-area relations, but does not intersect the same-stress relation.

The physical interpretation of the critical eccentricity is illustrated schematically in Fig. 7, where, as an example, the cross sections for the critical eccentricities are shown for the ratio $h_c/R_c = 0.15$ and the points of penetration of the inner surfaces of the cross sections are encircled. This ratio is quite large compared with the ones normally used in practical construction, but it has been chosen to emphasize the meaning of the critical eccentricities of the cross sections. Looking at Fig. 7 it can be noted that although the penetration behavior for all three VTE cylinder designs occurs at the flatter portion of the cross section, for the CTE cylinder penetration occurs at the more curved portion. The intersections in Fig. 6 of the relations for the same-load VTE cylinder and the CTE cylinder and of the relations for the same-area VTE cylinder and the CTE cylinder simply mean that there exists particular values of $h_c/R_c$ such that the penetration behavior of the two cylinders corresponding to the two intersecting curves happens for the same value of assigned eccentricity. Referring to Fig. 6, it is evident that when the ratio $h_c/R_c$ is small, as happens for the most of the cases of practical interest, the critical eccentricities are very close to unity. Moreover, from Fig. 7, when the eccentricity approaches the critical value, the walls of the VTE cylinder become so thick that some of the assumptions embedded in Eq. (1) are no longer valid. Based on those

**Table 1 Values of $\alpha$ and the variation of the thickness for the three designs**

| Design | $\alpha$ | $h(t)/h_c$ |
|---|---|---|
| Same-stress | 1 | $R(t)/R_c$ |
| Same-load | $1/g(e_0)$ | $R(t)/(R_c g(e_0))$ |
| Same-area | $1/g^2(e_0)$ | $R(t)/(R_c g^2(e_0))$ |

**Table 2 Dimensionless functions for determining the critical eccentricity for various cylinders**

| | |
|---|---|
| CTE | $2(1-e_0^2)/\mathcal{E}(e_0^2)$ |
| VTE, same-stress | $2(1-e_0^2)$ |
| VTE, same-load | $2(1-e_0^2)g(e_0)$ |
| VTE, same-area | $2(1-e_0^2)g^2(e_0)$ |

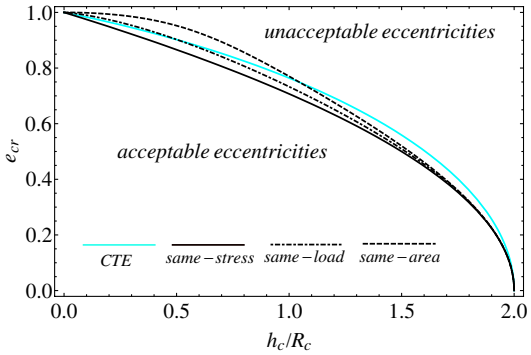


**Fig. 6 Critical eccentricity vs $h_c/R_c$ for various cylinders.**

arguments, it can be concluded that the critical eccentricity is a pure geometric limit and is not of practical interest.

Before closing this section it is interesting to make a comparison among the values that the three ratios $\sigma_{\mathrm{VTE}}/\sigma_{\mathrm{CTC}}$, $P_{\mathrm{VTE}}/P_{\mathrm{CTC}}$, and $A_{\mathrm{VTE}}/A_{\mathrm{CTC}}$ assume in each of the three designs of interest. These comparisons are summarized in Table 3. Keeping in mind that $g(e_0)$ is always greater than the unity, it should be noted that:

1) For the VTE cylinder, the same-stress design produces a buckling load and a cross-sectional area larger than those of the original CTC cylinder.

2) For the VTE cylinder, the same-load design produces a smaller buckling stress and a larger cross-sectional area than those of the original CTC cylinder.

3) For the VTE cylinder, the same-area design produces a smaller buckling stress and buckling load than those of the original CTC cylinder.

All the ratios in Table 3 vary monotonically with the eccentricity through the dimensionless function $g(e_0)$.

Finally, it is useful to explicitly derive analytical expressions for the axial stress resultant $N$. The axial stress resultant is defined as the integral of the axial stress through the thickness of the cylinder wall. It can be defined here as the product of the axial stress and the cylinder thickness. In Table 4 analytical expressions for the ratio between the axial stress resultants of the VTE cylinder and the original CTC cylinder, namely $N_{\mathrm{VTE}}/N_{\mathrm{CTC}}$, are given for all the three designs. These expressions are obtained multiplying member by member the last column of Table 1 and the first column of Table 3.

**Table 3 Values of three key ratios for the three designs**

| Design | $\sigma_{\mathrm{VTE}}/\sigma_{\mathrm{CTC}}$ | $P_{\mathrm{VTE}}/P_{\mathrm{CTC}}$ | $A_{\mathrm{VTE}}/A_{\mathrm{CTC}}$ |
|---|---|---|---|
| Same-stress | 1 | $g^2(e_0)$ | $g^2(e_0)$ |
| Same-load | $1/g(e_0)$ | 1 | $g(e_0)$ |
| Same-area | $1/g^2(e_0)$ | $1/g^2(e_0)$ | 1 |

**Table 4 Analytical expressions for axial-stress-resultant ratios for the three designs**

| Design | $N_{\mathrm{VTE}}/N_{\mathrm{CTC}}$ |
|---|---|
| Same-stress | $R(t)/R_c$ |
| Same-load | $R(t)/(R_c g^2(e_0))$ |
| Same-area | $R(t)/(R_c g^4(e_0))$ |

## V. Numerical Validation of the Proposed Designs

In this section the three VTE cylinder designs proposed in the previous section will be further studied using numerical results computed with the general-purpose finite element code ABAQUS® [26]. In particular, the results from ABAQUS will be compared with the results from the analytic predictions developed in the previous section. Because the analytic predictions are based on a rather simple premise, which does not consider prebuckling rotations or stresses other than the axial stress, such comparisons will be informative. Geometrically nonlinear prebuckling finite element analyses will be employed, and the results for S1 simply-supported boundary conditions [6] will be considered. The buckling condition will be identified by applying to one end of each cylinder the smallest axial compressive displacement that causes the tangent stiffness matrix of the numerical analysis to become singular. The stress state for this condition, in particular the axial stress level, will be considered the buckling stress. The cylinder responses of interest at this level of displacement will be compared with the respective analytic predictions for three values of assigned eccentricity, $e_0 = 0.50, 0.70$, and 0.85, as considered in Fig. 3, and two cylinder sizes in order to check the generality of the findings of the previous section. So-called small and large circular aluminum cylinders with the geometrical dimensions and the constitutive properties listed in Table 5 will be considered as the original CTC cylinders for the two sizes. In addition to the increased overall size of the large cylinder, the large cylinder is more flexible than the small cylinder in terms of wall thickness to radius ratio. The dimensions in Table 5 are within the range of values for which Eq. (1) is valid [4]. Using Eq. (11) the major and the minor radii $a$ and $b$ for the three different values of the eccentricity $e_0$ can be evaluated for both small and large cylinders. These values are listed in Table 6 along with the ratios of the minor to major radii and the values of the four functions appearing in Table 3.

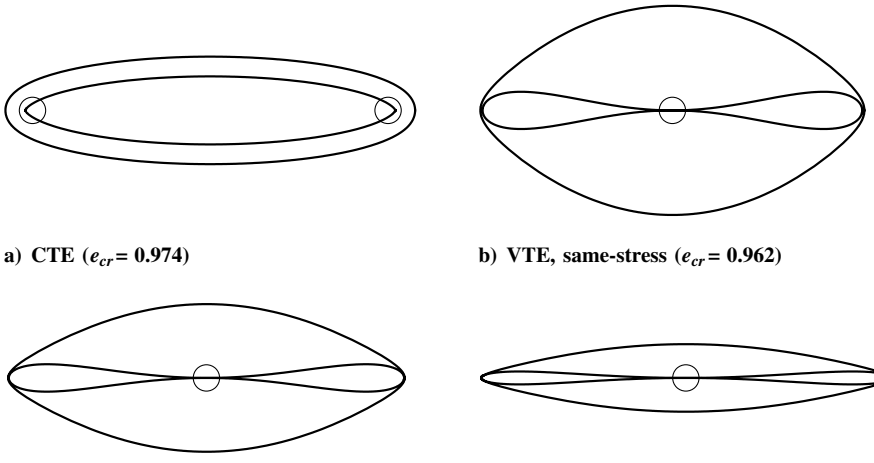

**a) CTE ($e_{cr}$ = 0.974)** **b) VTE, same-stress ($e_{cr}$ = 0.962)**

**c) VTE, same-load ($e_{cr}$ = 0.982)** **d) VTE, same-area ($e_{cr}$ = 0.997)**

**Fig. 7 Cross sections of critical eccentricity for $h_c/R_c = 0.15$ with points of penetrations of the inner surfaces encircled.**

**Table 5 Geometric and material properties used in the calculations for small and large CTC cylinders**

| | $R_c$ | $L_c$ | $h_c$ | $E$ | $\nu$ |
|---|---|---|---|---|---|
| Small | 0.1 m | 0.32 m | 1.12 mm | 70 GPa | 0.3 |
| Large | 0.5 m | 1.60 m | 2.24 mm | 70 GPa | 0.3 |

The finite element mesh employs 81 equispaced nodes in the axial direction and 168 equispaced nodes in the circumferential direction, for a total of 13,440 elements. An S4R four-node shell element from the ABAQUS library is used. This element uses thick-shell theory as the shell thickness increases and becomes a Kirchhoff thin-shell element as the thickness decreases. The thickness of each element will be assumed constant and equal to the thickness that the analytical function Eq. (15) assumes at the middle point of the element. In Fig. 8 a comparison between the actual area of a generic sector of the cross section associated with an element (black) and the area used in the numerical calculations (light gray) is shown. The superposition of the two different areas is filled in dark gray. As the number of nodes $M$ in the circumferential direction increases to 168, and consequently the circumferential length of each element decreases, the error in the representation of the cylinder cross-sectional area decreases. Specifically, the ratio between the cross-sectional area of the mesh for the VTE cylinder and the cross-sectional area of the mesh for the original CTC cylinder can be expressed as follows:

$$\frac{A_{\text{VTE}}}{A_{\text{CTC}}} = \frac{1}{Mh_c}\sum_{i=1}^{M} h(t_i) \tag{24}$$

where $t_i$ is the solution of the transcendental equation

$$\int_0^{t_i} \left|\frac{\mathrm{d}\mathbf{v}(t)}{\mathrm{d}t}\right| \mathrm{d}t = \left(i - \frac{1}{2}\right)\frac{2\pi R_c}{M} \qquad i = 1 \ldots M \tag{25}$$

In Tables 7–9 the values that Eq. (24) assumes for $M = 12$, 42, and 168 for the same-stress, -load, and -area designs and the three

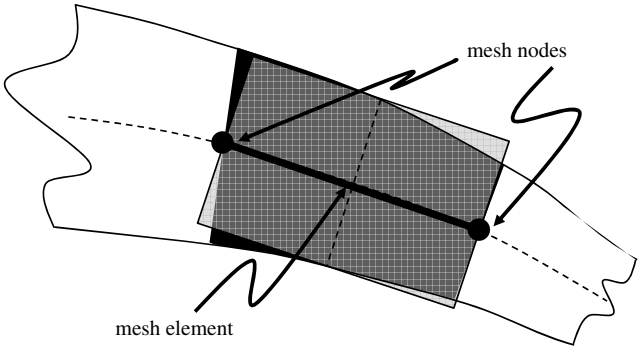


**Fig. 8 Comparison between the actual area and the numerically computed area of a sector of cross section.**

eccentricities of interest are shown. In the last column of the tables the analytic prediction is given (see Table 3, last column). For all three designs and for $M = 168$ the ratio $A_{\text{VTE}}/A_{\text{CTC}}$ converges to the analytic prediction to within 1% error. The accuracy slowly degenerates as the eccentricity increases.

Before discussing the VTE cylinders it is informative to consider the variation of the axial stress around the circumference of the CTE cylinders. In Figs. 9a and 9b the axial stress at the buckling condition as computed by ABAQUS for small and large CTE cylinders with the three values of eccentricity and normalized by the critical stress of the CTC cylinder are plotted as a function of the normalized circumferential location $s/2\pi R_c$ (see Fig. 2). For reference the normalized critical stress of the CTC cylinder, which is unity, is also plotted. From the figures it is first observed that the finite element analyses predict that the axial stress for CTE cylinders varies with circumferential position. The degree of the variation depends on the assigned eccentricity $e_0$ and the size of the cylinder. Most of the variation occurs in the flatter portions of the cross section, $s/(2\pi R_c) = 0.25, 0.75$, where the stress level is equal to the buckling stress. The variation is less for the large cylinder due to a lower value

**Table 6 Numerical values of geometric parameters for small and large VTE cylinders and three values of eccentricity**

| $e_0$ | Small | | Large | | $b/a$ | $g(e_0)$ | $1/g(e_0)$ | $g^2(e_0)$ | $1/g^2(e_0)$ |
|---|---|---|---|---|---|---|---|---|---|
| | a | b | a | b | | | | | |
| 0.50 | 0.1070 | 0.0927 | 0.5350 | 0.4635 | 0.87 | 1.0116 | 0.9886 | 1.0233 | 0.9772 |
| 0.70 | 0.1159 | 0.0827 | 0.5795 | 0.4135 | 0.71 | 1.0621 | 0.9415 | 1.1281 | 0.8865 |
| 0.85 | 0.1279 | 0.0674 | 0.6395 | 0.3370 | 0.53 | 1.2123 | 0.8249 | 1.4697 | 0.6804 |

**Table 7 Convergence of the area ratio $A_{\text{VTE}}/A_{\text{CTC}}$ for finite element analysis of same-stress design**

| $e_0$ | Finite element analysis | | | | | | Analytic prediction |
|---|---|---|---|---|---|---|---|
| | $M = 12$ | | $M = 42$ | | $M = 168$ | | $\frac{A_{\text{VTE}}}{A_{\text{CTC}}} = g^2(e_0)$ |
| | Small | Large | Small | Large | Small | Large | |
| 0.50 | 1.02225 | 1.02225 | 1.02321 | 1.02321 | 1.02329 | 1.02329 | 1.02329 |
| 0.70 | 1.03096 | 1.12230 | 1.12758 | 1.12758 | 1.12803 | 1.12803 | 1.12806 |
| 0.85 | 1.04310 | 1.44769 | 1.46792 | 1.46792 | 1.46959 | 1.46959 | 1.46970 |

**Table 8 Convergence of the area ratio $A_{\text{VTE}}/A_{\text{CTC}}$ for finite element analysis of same-load design**

| $e_0$ | Finite element analysis | | | | | | Analytic prediction |
|---|---|---|---|---|---|---|---|
| | $M = 12$ | | $M = 42$ | | $M = 168$ | | $\frac{A_{\text{VTE}}}{A_{\text{CTC}}} = g(e_0)$ |
| | Small | Large | Small | Large | Small | Large | |
| 0.50 | 1.01055 | 1.01055 | 1.01149 | 1.01149 | 1.01157 | 1.01157 | 1.01158 |
| 0.70 | 1.01916 | 1.05668 | 1.06165 | 1.06165 | 1.06207 | 1.06207 | 1.06210 |
| 0.85 | 1.03116 | 1.19416 | 1.21084 | 1.21084 | 1.21222 | 1.21222 | 1.21231 |

**Table 9 Convergence of the area ratio $A_{VTE}/A_{CTC}$ for finite element analysis of same-area design**

| $e_0$ | Finite element analysis | | | | | | Analytic prediction |
|---|---|---|---|---|---|---|---|
| | $M = 12$ | | $M = 42$ | | $M = 168$ | | $\frac{A_{VTE}}{A_{CTC}} = 1$ |
| | Small | Large | Small | Large | Small | Large | |
| 0.50 | 0.99898 | 0.99898 | 0.99991 | 0.99992 | 0.99999 | 0.99999 | 1 |
| 0.70 | 1.00749 | 0.99490 | 0.99957 | 0.99957 | 0.99997 | 0.99997 | 1 |
| 0.85 | 1.01935 | 0.98503 | 0.99879 | 0.99879 | 0.99992 | 0.99992 | 1 |

of the ratio $h/R$. In Table 10 both the circumferentially averaged magnitude and the circumferentially averaged normalized magnitude of the axial stress of the CTE cylinders at the buckling condition as computed from the finite element results of Fig. 9 are reported. In the same table the ratio of buckling stress for the CTE cylinder relative to the CTC cylinder, $\sigma_{CTE}/\sigma_{CTC}$, from the analytic prediction (Eq. (14) and Fig. 3) is reported. Although the finite element calculations show the axial stress in the CTE cylinders to vary somewhat with circumferential position, considering the average axial buckling stress from the finite element calculations for the CTE cylinders in that ratio (i.e., $\bar{\sigma}_{CTE}/\sigma_{CTC}$) it is seen from the table that the analytic predictions of Eq. (14) are no more than 10% different than the finite element calculations of that ratio. Similarly, the buckling loads computed by the finite element model for the CTE cylinders are reported in Table 11. Both the absolute and the normalized values are given. From Tables 10 and 11 it can be concluded that the buckling capacity of a CTE cylinder does decrease considerably with respect the CTC cylinder as the eccentricity increases, and Eq. (14) accurately predicts the decrease.

In what follows, the stresses, force resultants, and loads computed by ABAQUS for the CTE and VTE cylinders for the three different designs are presented and compared with like quantities from the analytic predictions.

**Table 10 Circumferentially averaged axial stress at the buckling condition for small and large CTE cylinders and three values of eccentricity**

| $e_0$ | Finite element analysis | | | | Analytic prediction |
|---|---|---|---|---|---|
| | $\bar{\sigma}_{CTE}$, MPa | | $\bar{\sigma}_{CTE}/\sigma_{CTC}$ | | Eq. (14) |
| | Small | Large | Small | Large | |
| 0.50 | 352.59 | 140.21 | 0.8567 | 0.8404 | 0.8090 |
| 0.70 | 274.03 | 107.61 | 0.6659 | 0.6550 | 0.6163 |
| 0.85 | 186.58 | 72.65 | 0.4534 | 0.4355 | 0.4118 |

**Table 11 Axial load at the buckling condition for small and large CTE cylinders and three values of eccentricity**

| $e_0$ | Finite element analysis | | | | Analytic prediction |
|---|---|---|---|---|---|
| | $P_{CTE}$, N | | $P_{CTE}/P_{CTC}$ | | Eq. (14) |
| | Small | Large | Small | Large | |
| 0.50 | 248121 | 98670 | 0.8567 | 0.8404 | 0.8090 |
| 0.70 | 192842 | 75730 | 0.6659 | 0.6550 | 0.6163 |
| 0.85 | 131298 | 55130 | 0.4534 | 0.4355 | 0.4118 |

### A. Same-Stress Design

In Fig. 10 the circumferential variations of the normalized axial stress for the same-stress design VTE cylinders at the buckling condition are shown. Results for small and large cylinders with the three levels of eccentricity are illustrated by way of subfigures. Each subfigure includes the axial stress for the VTE cylinder at the buckling condition from the analytic prediction (horizontal straight line) and the axial stress for the same VTE cylinder at the buckling condition as computed by the finite element analysis. As a reference, the axial stress for the CTE cylinder at the buckling condition from Fig. 9 is also included in each subfigure. From Fig. 10 it is observed that the finite element analysis predicts that the axial stress for the VTE cylinders varies with circumferential position, as is the case for CTE cylinder but in contrast to the circumferentially uniform stress state of the analytic prediction. The degree of circumferential variation depends again on the assigned eccentricity $e_0$ and the size of the cylinder. It appears that the analytic prediction provides a reasonable estimate of the performance of the VTE cylinder. This is definitely the case for $e_0 = 0.50$ and in an average sense for $e_0 = 0.70$. For $e_0 = 0.85$ the developed analysis overpredicts the average of the finite element model by about 5% for small and 2% for large cylinders. Furthermore, a $\pm 5\%$ variation of axial stress around the circumference of the small cylinders is predicted by the finite element model for $e_0 = 0.85$. For the large cylinders with $e_0 = 0.85$ the variation is less. For clamped boundary conditions (not shown), the stress variation around the circumference for the small VTE cylinder is about $\pm 2.5\%$ and the average of the finite element model is within 2.5% of the analytical prediction. Further quantitative comparisons regarding the stresses are made in Table 12 with the tabulation of key ratios of average axial stresses at the buckling

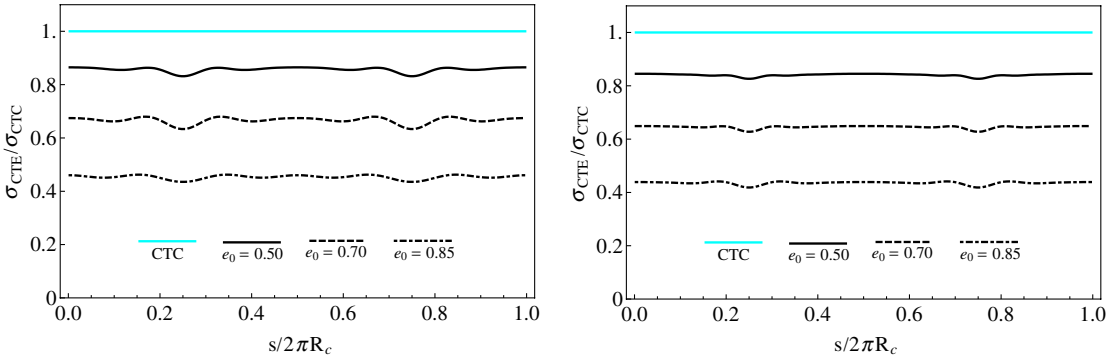


a) Small b) Large

**Fig. 9 Circumferential variation of axial stress at the buckling condition for small and large CTC and CTE cylinders and three values of eccentricity.**

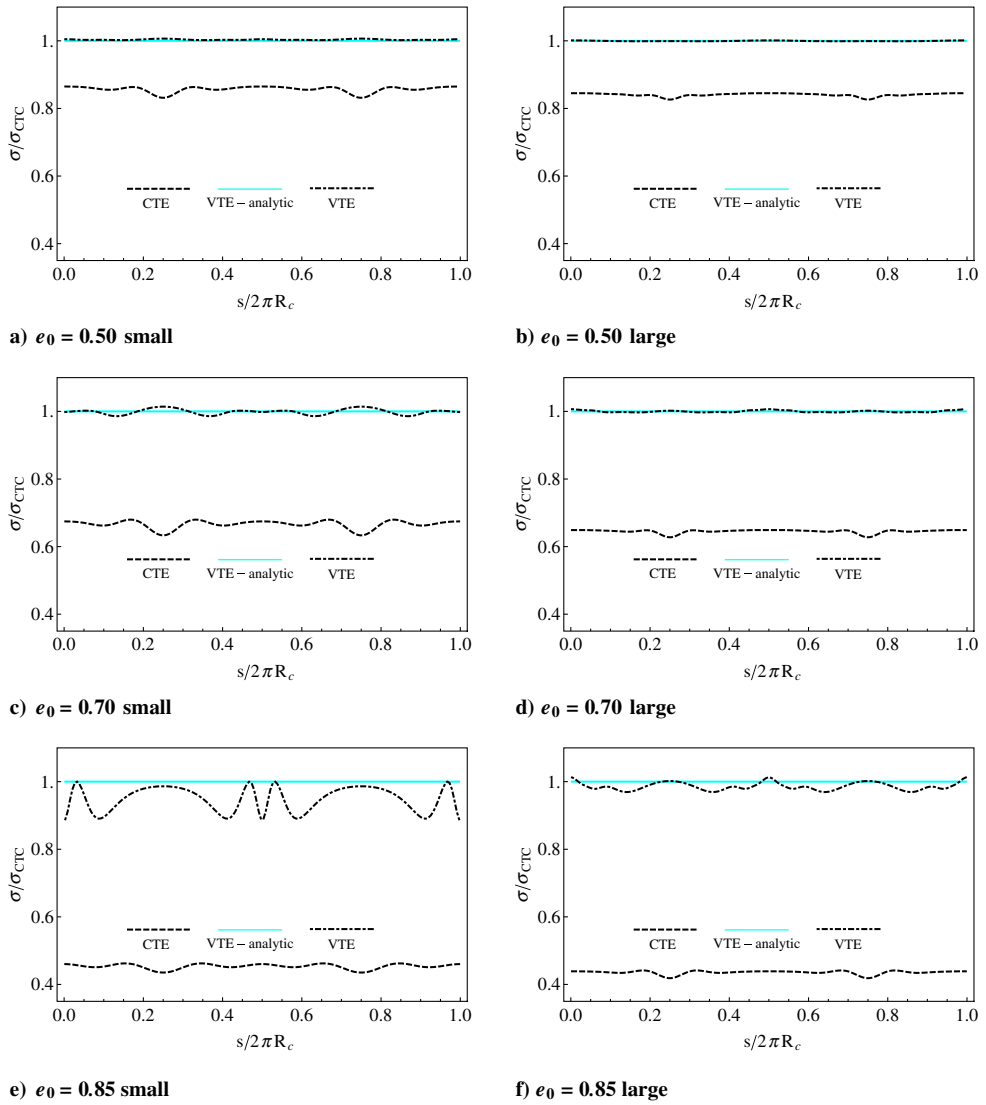


**Fig. 10 Comparison among the axial stresses at the buckling condition for small and large VTE and CTE cylinders for three values of eccentricity and same-stress design.**

condition as computed from finite element analyses and as determined from the analytic prediction. The ratio between $\bar{\sigma}_{\mathrm{VTE}}$ and $\bar{\sigma}_{\mathrm{CTE}}$ is a measure of the increase in the axial stress at the buckling condition obtained by tailoring the thickness of the elliptical cylinder relative to keeping the thickness of the elliptical cylinder uniform. As seen, this increase varies from about 17% for a small cylinder with $e_0 = 0.50$ to more that 100% for a large cylinder with $e_0 = 0.85$. The ratio between $\bar{\sigma}_{\mathrm{VTE}}$ and $\sigma_{\mathrm{CTC}}$ is a measure of the axial stress at the buckling condition of the thickness-tailored elliptical cylinder relative to the axial stress at the buckling condition of the original circular cylinder. For all cases the ratio between $\bar{\sigma}_{\mathrm{VTE}}$ and $\sigma_{\mathrm{CTC}}$ is very close to the unit value, emphasizing the fact that the buckling stress of the original circular cylinder is, essentially, fully recovered. Because with the developed analysis the stress does not vary with circumferential position, $\bar{\sigma}_{\mathrm{VTE}}/\sigma_{\mathrm{CTC}}$ is also of unit value for the analytic prediction. For comparison this unit value from the analytic prediction of Table 3 is included in the last column of Table 12. For a clamped boundary condition the numbers are similar to those of the simply supported condition, except that the gain obtained by tailoring is computed to be somewhat greater. A comparison of load ratios at the buckling condition is presented in Table 13. The ratio $P_{\mathrm{VTE}}/P_{\mathrm{CTE}}$ is a measure of the gain in axial load capability obtained by tailoring the thickness of the elliptical cylinder relative to keeping the thickness of the elliptical cylinder uniform. This gain varies from about 20% for the small cylinder with $e_0 = 0.50$ to more than 200% for the large cylinder with $e_0 = 0.85$. The ratio $P_{\mathrm{VTE}}/P_{\mathrm{CTC}}$ is a measure of the gain in axial load capability of the thickness-tailored elliptical cylinder relative to the original circular cylinder. As seen, the ratio is above one, and so there is clearly a gain relative to the original circular cylinder. It is also seen that the ratio $P_{\mathrm{VTE}}/P_{\mathrm{CTC}}$ is described quite accurately by $g^2(e_0)$, as predicted in Table 3. As observed, the critical load of the VTE cylinder increases with respect to the CTC cylinder as the eccentricity increases.

It should be remarked that with the same-stress design the improvement in the buckling capacity of the VTE cylinder is due in part to an increment in cross-sectional area, also related to $g^2(e_0)$ (see

**Table 12 Comparison among key stress ratios at the buckling condition for small and large VTE and CTE cylinders and three values of eccentricity, same-stress design, finite element analysis, and analytic prediction**

| $e_0$ | Finite element analysis | | | | Analytic prediction |
|---|---|---|---|---|---|
| | $\bar{\sigma}_{\mathrm{VTE}}/\bar{\sigma}_{\mathrm{CTE}}$ | | $\bar{\sigma}_{\mathrm{VTE}}/\sigma_{\mathrm{CTC}}$ | | $\frac{\sigma_{\mathrm{VTE}}}{\sigma_{\mathrm{CTE}}} = 1$ |
| | Small | Large | Small | Large | |
| 0.50 | 1.1715 | 1.1894 | 1.0036 | 0.9996 | 1 |
| 0.70 | 1.5003 | 1.5504 | 0.9990 | 1.0001 | 1 |
| 0.85 | 2.0903 | 2.2641 | 0.9489 | 0.9860 | 1 |

**Table 13 Comparison among key load ratios at the buckling condition for small and large VTE and CTE cylinders and three values of eccentricity, same-stress design, finite element analysis, and analytic prediction**

| $e_0$ | Finite element analysis | | | | Analytic prediction |
|---|---|---|---|---|---|
| | $P_{VTE}/P_{CTE}$ | | $P_{VTE}/P_{CTC}$ | | $\frac{P_{VTE}}{P_{CTC}} = g^2(e_0)$ |
| | Small | Large | Small | Large | |
| 0.50 | 1.1988 | 1.2170 | 1.0271 | 1.0228 | 1.0233 |
| 0.70 | 1.6935 | 1.7480 | 1.1277 | 1.1275 | 1.1281 |
| 0.85 | 3.0990 | 3.3261 | 1.4050 | 1.4485 | 1.4697 |

Tables 3 and 6). However, the distribution of the area (i.e., varying the thickness with circumferential location) has a major role in the improvement in buckling capability. This is evident by realizing that although the ratio $P_{VTE}/P_{CTE}$ shows over a 200% gain for both the small and the large cylinders with $e_0 = 0.85$ (i.e., $P_{VTE}/P_{CTE} = 3.3261$ for the large cylinder), the area has increased by only 47% (i.e., $A_{VTE}/A_{CTE} = 1.4697$, see Tables 3 and 6).

The variation of the axial stress resultant, $N$, with circumferential location at the buckling condition as predicted by the finite element analysis is shown in Fig. 11. The analytic prediction from Table 4 for the VTE cylinder is also illustrated in the figures. The stress resultants are normalized by the stress resultant for the CTC cylinder $N_{CTC}$. For reference purposes the stress resultant for the CTC cylinder $N_{CTC}$ is included and is the horizontal line at unity. At first glance it is clear from Fig. 11 that, importantly, for all cases the analytic prediction of the $N$ vs $s$ relation is almost indistinguishable from the finite element calculations. Looking at more detail it is observed that although the stress resultant for the CTE cylinder $N_{CTE}$ is nearly uniform around the circumference and always less than the stress resultant for the CTC cylinder, the stress resultant for the VTE cylinder $N_{VTE}$ has considerable amplitude modulation, being largest in the flatter regions of the elliptical cross section in all cases. This follows because the amplitude of $N$ should be proportional to the thickness of the shell due to the proposed design that forces the stress to be uniform with circumferential location. It should be noted that $N_{VTE}$ intersects $N_{CTC}$ where the radius of curvature of the ellipse is equal to the radius of original circle, $R_c$. The area under the relationship for $N$ vs $s$ is the total axial load. From a qualitative inspection of Fig. 11 it is quite evident that for each case the area under the $N_{CTE}$ relation is less the area under the other two relations. Moreover, the average value of $N_{VTE}$ (not shown in the figure) seems to have a positive offset relative to $N_{CTC}$, particularly for large values of eccentricities and, for sure, relative to $N_{CTE}$. Consequently, as has been pointed out in previous tables, the axial buckling load of the VTE cylinder is greater than the axial buckling load of the CTE cylinder.

### B. Same-Load Design

Comparing Fig. 12 with Fig. 10 and Fig. 13 with Fig. 11 it can be concluded that the overall characteristics of the stress and stress-

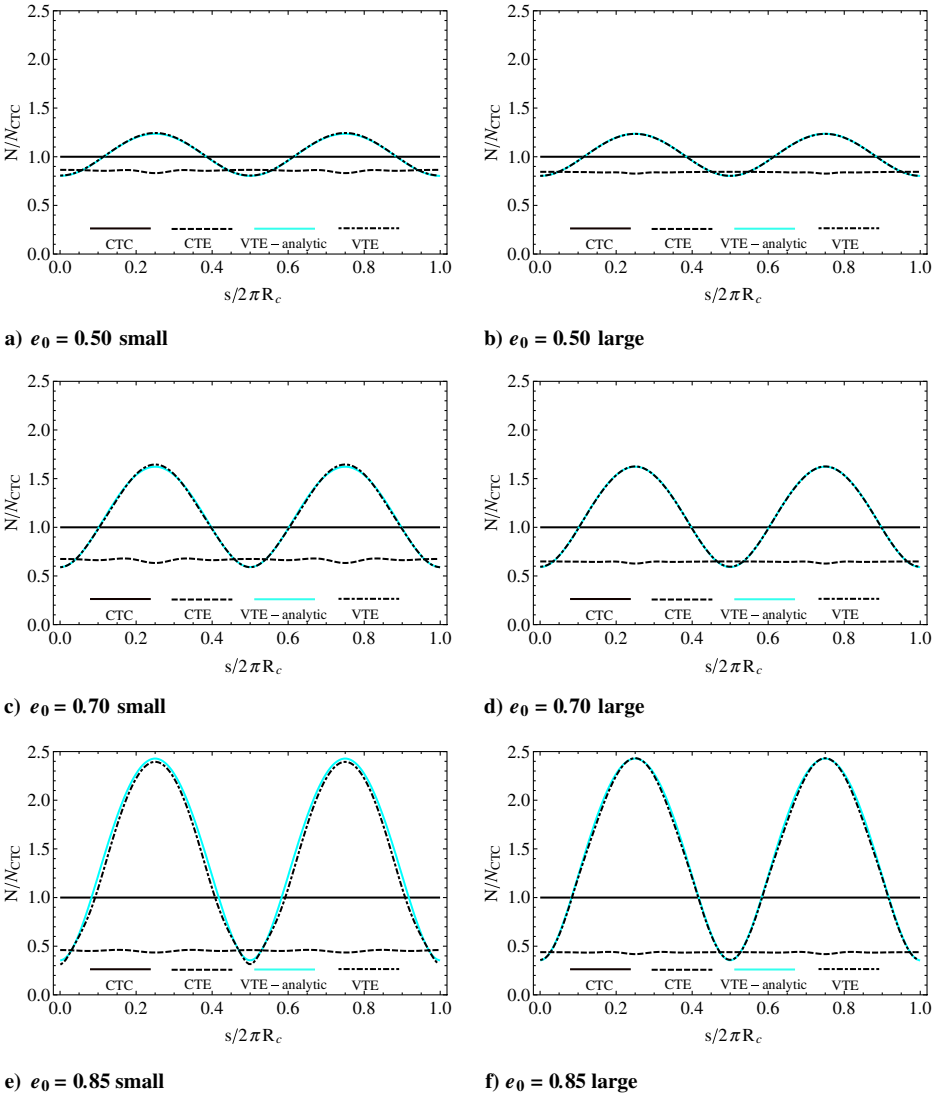


**Fig. 11 Comparison among the stress resultants at the buckling condition for small and large VTE and CTE cylinders and three values of eccentricity and same-stress design.**

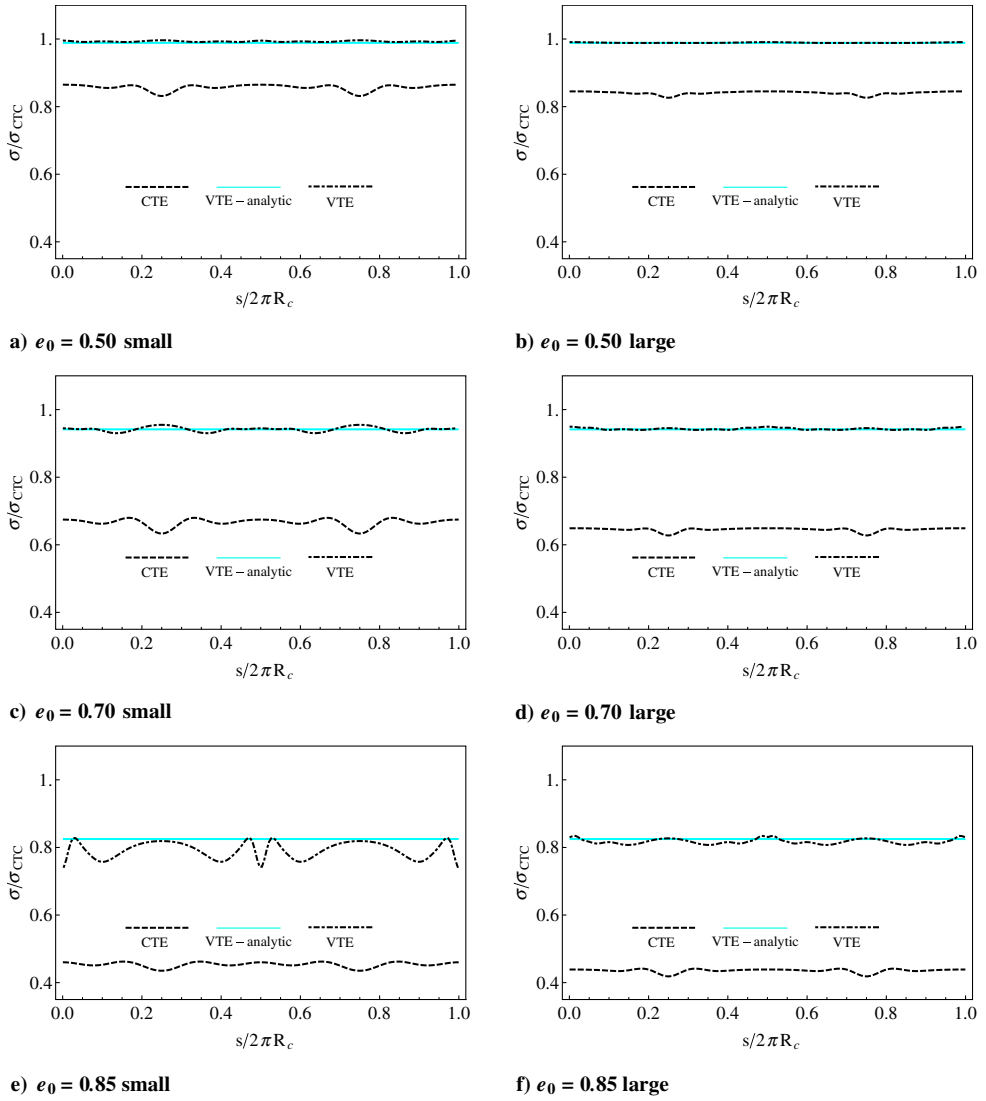


**Fig. 12 Comparison among the axial stresses at the buckling condition for small and large VTE and CTE cylinders and three values of eccentricity and same-load design.**

resultant variation with circumferential location for the same-load designs are similar to the characteristics of those responses for the same-stress designs. Additionally, the correlations between the analytically predicted stresses and stress resultants for the same-load design VTE cylinders and the like response as computed by the finite element model are generally good, but with less correlation between the stress levels for both small and large cylinders for the case of eccentricity $e_0 = 0.85$. There are, however, differences between the same-load and same-stress designs. The most obvious difference between designs in the variations of stress with circumferential location, Figs. 10 and 12, is that the normalized stress levels for the same-load design VTE cylinders, as predicted by both the developed analysis and the finite element model, are lower than for the same-stress design. The same is true of the stress-resultant levels of the same-load design, Fig. 13, as compared with those of the same-stress design, Fig. 11. This trend is particularly evident for the case of large eccentricities, where in Fig. 12 for both small and large same-load design VTE cylinders with $e_0 = 0.85$ the normalized stress level is near 0.8, as opposed to a value near unity for both small and large same-stress design VTE cylinders with eccentricity $e_0 = 0.85$ in Fig. 10. Likewise, for both small and large cylinders with eccentricity $e_0 = 0.85$, the peak loads of the normalized stress resultants for the same-stress designs in Fig. 11 are close to 2.5 for both small and large cylinders, whereas for the same-load designs in Fig. 13, the peak levels are about 1.7. A review of Table 13 reveals that for the same-stress design the ratio of $P_{\mathrm{VTE}}/P_{\mathrm{CTC}}$ is greater than unity, and increases with increasing eccentricity, meaning that the buckling load of the VTE cylinder is greater than the buckling load of the original CTC cylinder. For this ratio to be unity, as is required for the same-load design, meaning that the buckling loads are the same, does not require as high a stress level for the VTE cylinders; hence, the lower levels of stress and stress resultants for the same-load design. The lower stress levels for the same-load design are reflected in all the stress ratios of Table 14 as compared with those of Table 12, and the load ratios of Table 15 as compared with those of Table 13. Regarding the lower level of stress for the same-load design, because $\sigma_{\mathrm{VTE}}/\sigma_{\mathrm{CTC}}$ (and, hence, $\bar{\sigma}_{\mathrm{VTE}}/\sigma_{\mathrm{CTC}}$) is given as $1/g(e_0)$ by the analytic prediction, and because $g(e_0)$ is greater than one, the lower value of stress for the same-load design must be expected. It is observed from Table 14 that the value of $1/g(e_0)$ correlates well with the value of $\bar{\sigma}_{\mathrm{VTE}}/\sigma_{\mathrm{CTC}}$ as computed by the finite element analysis, particularly for the large cylinders.

The ratios $\bar{\sigma}_{\mathrm{VTE}}/\bar{\sigma}_{\mathrm{CTE}}$ and $P_{\mathrm{VTE}}/P_{\mathrm{CTE}}$ in Tables 14 and 15 respectively, again reflect the gain in varying the thickness of the cylinder wall with circumferential position in the elliptical cylinders. Some of this gain is due to an increment of area, as given by the values of $g(e_0)$ (see Tables 3 and 6), but again, most of the gain must be attributed to the redistribution of material by varying the thickness with circumferential location. For example, for $e_0 = 0.85$ the buckling load for the large VTE cylinder is over 100% greater then

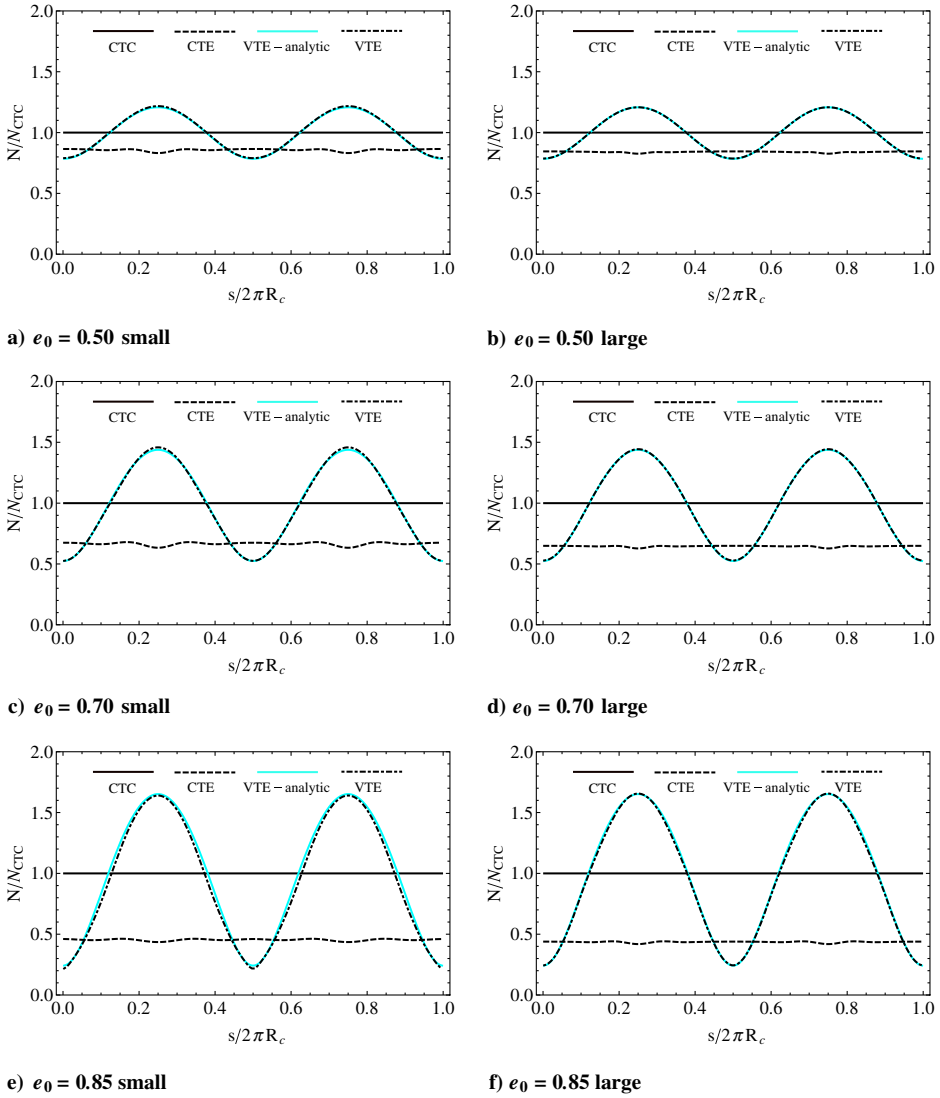


**Fig. 13 Comparison among the axial stress resultants at the buckling condition for small and large VTE and CTE cylinders for three values of eccentricity and same-load design.**

the buckling load for the large CTE cylinder (i.e., $P_{VTE}/P_{CTE}=2.2736$), whereas the area increase is only 21% (see values of $g(e_0)$ in Tables 3 and 6).

### C. Same-Area Design

The variations of the normalized stresses and stress resultants as a function of circumferential location for the same-area design VTE cylinders are illustrated in Figs. 14 and 15, respectively. Tables 14 and 15 provide information similar to Tables 12–15 for the same-stress and same-load designs, respectively.

By comparing Fig. 14 with Figs. 10 and 12 it is observed that for both small and large cylinders with $e_0 = 0.85$, for example, the normalized stress level around the circumference for the VTE cylinders has decreased from about unity for the same-stress designs, to about 0.8 for the same-load designs, to just below 0.7 for the same-area designs. Likewise, by comparing Fig. 15 with Figs. 11 and 13, it is observed that the peak value of the stress resultant for both small and large VTE cylinders with $e_0 = 0.85$ has decreased from about 2.5 for the same-stress designs, to about 1.7 for the same-load designs, to about 1.2 for the same-area designs. The correlation between the analytic predictions and the finite element analysis is again quite good for eccentricities $e_0 = 0.50$ and $e_0 = 0.70$, with less agreement for the case of $e_0 = 0.85$. The lower overall stress level for the same-area designs, compared with the other two designs, is

**Table 14 Comparison among key stress ratios at the buckling condition for small and large VTE and CTE cylinders and three values of eccentricity, same-load design, finite element analysis, and analytic prediction**

| $e_0$ | Finite element analysis | | | | Analytic prediction |
|---|---|---|---|---|---|
| | $\bar{\sigma}_{VTE}/\bar{\sigma}_{CTE}$ | | $\bar{\sigma}_{VTE}/\sigma_{CTE}$ | | $\frac{\sigma_{VTE}}{\sigma_{CTC}} = 1/g(e_0)$ |
| | Small | Large | Small | Large | |
| 0.50 | 1.1591 | 1.1770 | 0.9930 | 0.9891 | 0.9886 |
| 0.70 | 1.4143 | 1.4622 | 0.9417 | 0.9432 | 0.9415 |
| 0.85 | 1.7472 | 1.8773 | 0.7921 | 0.8175 | 0.8249 |

**Table 15 Comparison among key load ratios at the buckling condition for small and large VTE and CTE cylinders and three values of eccentricity, same-load design, finite element analysis, and analytic prediction**

| $e_0$ | Finite element analysis | | | | Analytic prediction |
|---|---|---|---|---|---|
| | $P_{VTE}/P_{CTE}$ | | $P_{VTE}/P_{CTC}$ | | $\frac{P_{VTE}}{P_{CTE}} = 1$ |
| | Small | Large | Small | Large | |
| 0.50 | 1.1726 | 1.1904 | 1.0046 | 1.0005 | 1 |
| 0.70 | 1.5029 | 1.5521 | 1.0007 | 1.0012 | 1 |
| 0.85 | 2.1285 | 2.2736 | 0.9650 | 0.9901 | 1 |

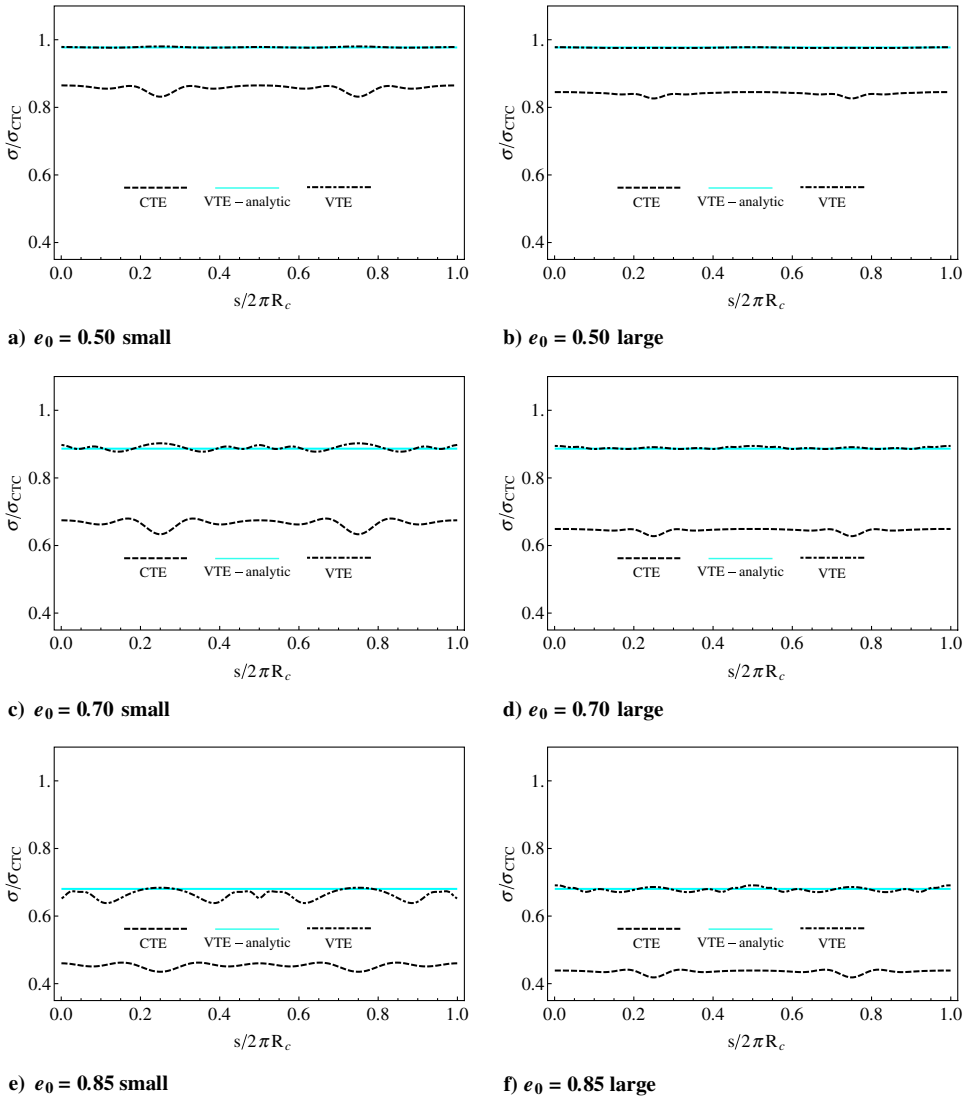


**Fig. 14 Comparison among the stresses at the buckling condition for small and large VTE and CTE cylinders for three values of eccentricity and same-area design.**

reflected in the entries of Tables 16 and 17 as compared with entries of Tables 12–15 for all three values of eccentricity. It is seen in Tables 16 and 17 that the ratios $\bar{\sigma}_{\mathrm{VTE}}/\sigma_{\mathrm{CTC}}$ and $P_{\mathrm{VTE}}/P_{\mathrm{CTC}}$ given by $1/g^2(e_0)$ from the analytic predictions correlate well with the finite element calculations. Furthermore, the fact that the ratio $P_{\mathrm{VTE}}/P_{\mathrm{CTE}}$ is greater than unity for all three values of eccentricity and both small and large cylinders for the same-area VTE designs unequivocally verifies the gain in redistributing the area in the elliptical cylinders. Specifically, from Table 17 for the large same-area design VTE cylinders there is an increment of about 56% in the buckling load compared with the CTE cylinder for $e_0 = 0.85$. However, unlike the same-stress design VTE cylinders for which the ratio $P_{\mathrm{VTE}}/P_{\mathrm{CTC}}$ is greater than unity for all cases, and unlike the same-load design VTE cylinders for which the ratio $P_{\mathrm{VTE}}/P_{\mathrm{CTC}}$ is forced to be unity, for the same-area design VTE cylinders the ratio $P_{\mathrm{VTE}}/P_{\mathrm{CTC}}$ is less than unity, meaning that the same-area design VTE cylinders have buckling loads less than those of the original CTC cylinders.

Before closing this section, cylinder deformations should be discussed. The prebuckling deformations of small VTE cylinders for all three eccentricities are shown in Fig. 16. A few comments can be made by comparing Fig. 16b with Fig. 1. First, although for the CTE cylinder with $e_0 = 0.70$ shown in Fig. 1b the deformations are mainly localized within the flatter regions, for the VTE cylinder with the same value of eccentricity shown Fig. 16b the deformations

**Table 16 Comparison among key stress ratios at the buckling condition for small and large VTE and CTE cylinders and three values of eccentricity, same-area design, finite element analysis, and analytic prediction**

| $e_0$ | Finite element analysis | | | | Analytic prediction |
|---|---|---|---|---|---|
| | $\bar{\sigma}_{\mathrm{VTE}}/\bar{\sigma}_{\mathrm{CTE}}$ | | $\bar{\sigma}_{\mathrm{VTE}}/\sigma_{\mathrm{CTC}}$ | | $\frac{\sigma_{\mathrm{VTE}}}{\sigma_{\mathrm{CTC}}} = 1/g^2(e_0)$ |
| | Small | Large | Small | Large | |
| 0.50 | 1.1414 | 1.1618 | 0.9779 | 0.9764 | 0.9772 |
| 0.70 | 1.3356 | 1.3781 | 0.8893 | 0.8889 | 0.8865 |
| 0.85 | 1.4644 | 1.5593 | 0.6639 | 0.6790 | 0.6804 |

**Table 17 Comparison among key load ratios at the buckling condition for small and large VTE and CTE cylinders and three values of eccentricity, same-area design, finite element analysis, and analytic prediction**

| $e_0$ | Finite element analysis | | | | Analytic prediction |
|---|---|---|---|---|---|
| | $P_{\mathrm{VTE}}/P_{\mathrm{CTE}}$ | | $P_{\mathrm{VTE}}/P_{\mathrm{CTC}}$ | | $\frac{P_{\mathrm{VTE}}}{P_{\mathrm{CTC}}} = 1/g^2(e_0)$ |
| | Small | Large | Small | Large | |
| 0.50 | 1.1415 | 1.1616 | 0.9779 | 0.9762 | 0.9772 |
| 0.70 | 1.3361 | 1.3773 | 0.8896 | 0.8884 | 0.8865 |
| 0.85 | 1.4685 | 1.5570 | 0.6658 | 0.6781 | 0.6804 |

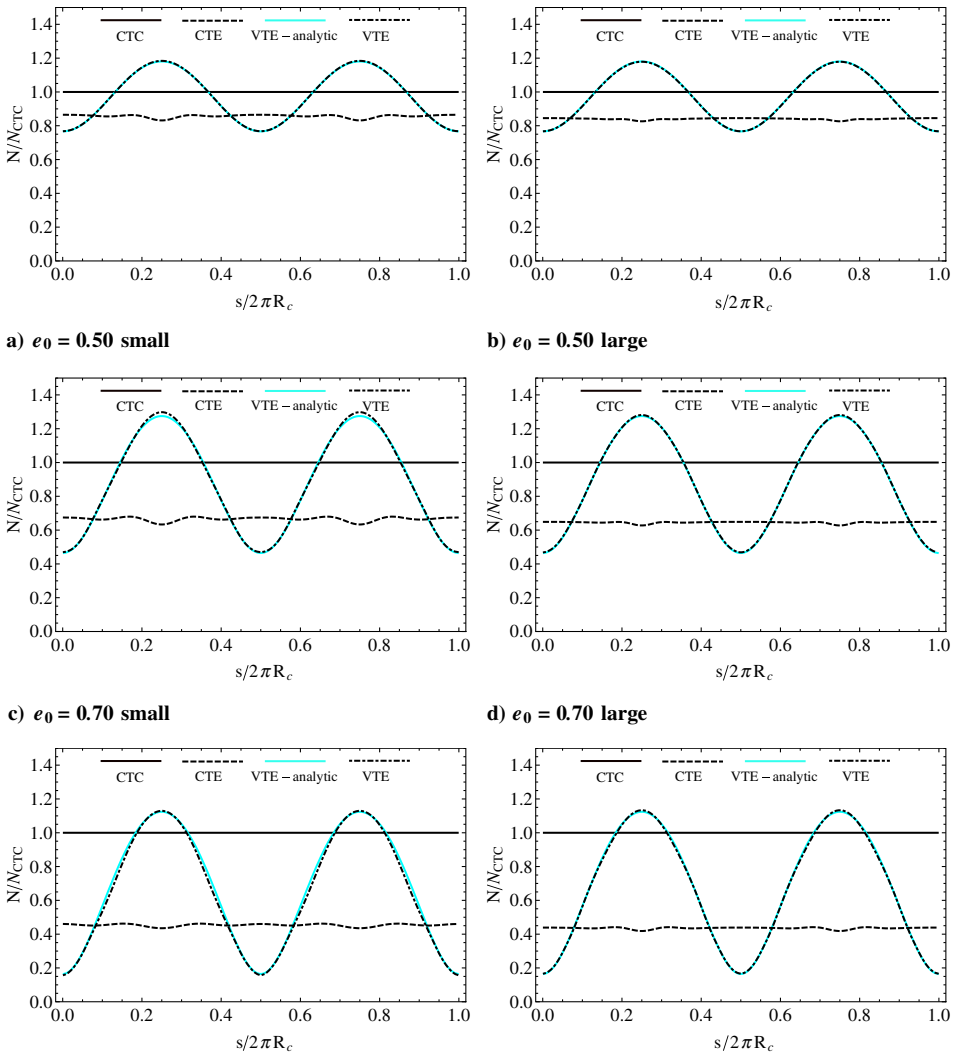


**Fig. 15 Comparison among the axial stress resultants at the buckling condition for small and large VTE and CTE cylinders for three values of eccentricity and same-area design.**

involve the entire circumference. Second, as happens for the CTC cylinder, the deformations are confined to boundary layers localized at the two ends of the cylinder. Third, an important difference between the deformations of the CTC cylinder shown in Fig. 1a and those of the VTE cylinder in Fig. 16b is that although the boundary layer for the former case has a uniform width around the circumference, for the latter case the width is modulated due to the variation of the curvature with circumferential location, the boundary layer being wider in the flatter regions and narrower in the more curved regions. From Fig. 16 it can be seen that all the comments previously made for $e_0 = 0.70$ apply to $e_0 = 0.50$ and $e_0 = 0.85$. The prebuckling deformed shapes associated with the same-load and -area designs (not shown) are qualitatively similar to the deformed shapes of the same-stress design shown in Fig. 16. The only difference that can be found is in the amplitude of the deformation that results due to the fact that the same-stress design allows a larger displacement before reaching the critical stress at the buckling condition as compared with the same-load and -area designs.

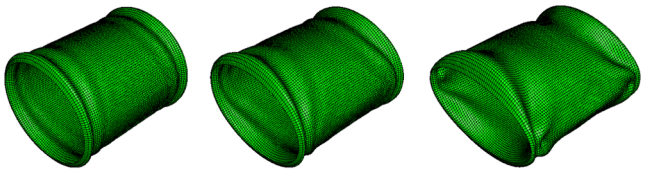

**a) $e_0 = 0.50$ b) $e_0 = 0.70$ c) $e_0 = 0.85$**

**Fig. 16 Deformed prebuckling shapes of axially loaded, small, simply supported VTE cylinders with three values of eccentricity, using same-stress design.**

## VI. Conclusions

Equation (1) is a simple relation derived for a homogeneous, isotropic circular cylinder with a uniform wall thickness, neglecting prebuckling rotations. This equation is applicable to noncircular cylinders, and predicts a loss of load capability for an elliptical cylinder with the same circumference and wall thickness as the circular cylinder. Here, Eq. (1) has been used to develop three designs to increase the axial buckling load capability of the elliptical cylinder by considering a nonuniform wall thickness. In fact, Eq. (1) has been used to specify the variation of wall thickness with circumferential position for the elliptical cylinder. Numerical results for the same-stress, same-load, and same-area designs developed with Eq. (1) as a guideline have been computed and compared with results obtained for a finite element analysis considering prebuckling rotations of these three designs. There are some differences between the finite element results and the analytic predictions based on Eq. (1). However, designing the variation of the wall thickness using finite elements is a cumbersome and time-consuming approach. In that context, Eq. (1) does well. Moreover, the results obtained using

Eq. (1) are good enough that conclusions can be drawn regarding tradeoffs in the designs. For example, and continuing with an earlier example, according to Fig. 3, which is based on Eq. (14) of the developed analysis, a simply-supported CTE cylinder with $e_0 = 0.70$ retains only 62% of the buckling load of the original CTC cylinder. This is collaborated in Table 11 where a buckling load retention of 67% rather than 62% is computed by the finite element analysis for the small cylinder. Both the analytic prediction and the finite element analysis for the small cylinder each illustrate that the same-area VTE design for the case of $e_0 = 0.70$ in Table 17 retains 89% of the buckling load of the CTC cylinder. This translates into better than a 30% increase in buckling load of the VTE cylinder compared with the CTE cylinder (i.e., $P_{\mathrm{VTE}}/P_{\mathrm{CTE}} = 1.3361$). Because the analytic prediction correlates so well with the finite element analysis, Table 15 can then be used to quickly conclude that the buckling load of the small VTE cylinder with $e_0 = 0.70$ can be made to retain 100% of the buckling load of the CTC cylinder by using the same-load design ($P_{\mathrm{VTE}}/P_{\mathrm{CTC}} = 1.0007$) if a 6% increase in weight can be tolerated (i.e., $g(0.70) = 1.0621$). If even more weight can be tolerated, Table 13 can be used to show that the same-stress design for the small VTE cylinder with $e_0 = 0.70$ further increases the buckling load to 113% of the CTC cylinder ($P_{\mathrm{VTE}}/P_{\mathrm{CTC}} = 1.1277$) with only slightly more than a 13% increase in weight (i.e., $g^2(0.70) = 1.1281$).

There are a number of issues to consider for future investigations of variable wall thickness designs. The role of imperfections is always an important topic with cylindrical structures. As mentioned in previous sections, several investigators reported reduced imperfection sensitivity with noncircular cylinders. However, with the variable-thickness elliptical cylinders studied here, imperfections at circumferential locations where the wall is thinner may be more important than for noncircular cylinders with uniform wall thickness. A study of the postbuckling behavior would also be important. For all cases considered here the stresses at buckling were less than the compressive yield stress of many aluminum alloys, particularly for the large cylinder. Therefore, snap-through and other large elastic deformations associated with postbuckling would be of interest. Finally, the manufacturing of variable-thickness elliptical cylinders should be considered so that experiments can be conducted to compare with the findings presented. Depending on the material and actual size of the cylinder, simply machining a block of material with numerically controlled equipment, though wasting considerable material, would be one approach. Alternatively, the cylinder could be made in two halves and the two halves joined by a process such as friction stir welding in the axial direction along the thinner portions of the cross section. Finally, it may be possible to develop a mold with a cavity the shape of the cross section and cast the cylinder while the cylinder material is in a liquid state.

## References


[1] Kempner, J., and Chen, Y. N., "Postbuckling of an Axially Compressed Oval Cylindrical Shell," *Proceedings of the XII International Congress of Applied Mechanics*, edited by M. Hetényi and W. Vincenti, Springer–Verlag, Berlin, 1969, pp. 246–256.

[2] Hutchinson, J. W., "Buckling and Initial Postbuckling Behavior of Oval Cylindrical Shells Under Axial Compression," *Journal of Applied Mechanics*, Vol. 35, No. 1, 1968, pp. 66–72.

[3] Brush, D., and Almroth, B., *Buckling of Bars, Plates, and Shells*, McGraw–Hill, New York, 1975, p. 168.

[4] Yamaki, N., *Elastic Stability of Circular Cylindrical Shells*, North-Holland, New York, 1984, pp. 84, 101–102.

[5] Kempner, J., and Chen, Y. N., "Buckling and Postbuckling of an Axially Compressed Oval Cylindrical Shell," *Proceedings–Symposium On Theory of Shells to Honor Lloyd Hamilton Donnell*, edited by D. M.-U. Houston, McCutchaw Publishing Corp., Houston, TX,1967, pp. 141–175.

[6] Jones, R., *Buckling of Bars, Plates, and Shells*, Bull Ridge Publishing, Blacksburg, VA 2006, p. 247.

[7] Fuchs, H., and Hyer, M., "Nonlinear Prebuckling Response of Short Thin-Walled Laminated Composite Cylinders in Bending," *Composite Structures*, Vol. 34, No. 3, 1996, pp. 309–324. doi:10.1016/0263-8223(95)00152-2

[8] Sun, M., and Hyer, M., "Use of Material Tailoring to Improve Buckling Capacity of Elliptical Composite Cylinders," *AIAA Journal*, Vol. 46, No. 3, 2008, pp. 770–782. doi:10.2514/1.32495

[9] Lundquist, E., and Burke, W. F., "Strength Tests of Thin-Walled Duraluminum Cylinders of Elliptical Cross Section," NACA TN 527, 1935.

[10] Heck, O. S., "The Stability of Orthotropic Elliptical Cylinders in Pure Bending," NACA TM 834, 1937.

[11] Marguerre, K., "Stability of Cylindrical Shell of Variable Curvature," NACA TM 1032, 1951.

[12] Kempner, J., and Chen, Y. N., "Large Deflections of an Axially Compressed Oval Cylindrical Shell," Polytechnic Institute of Brooklyn PIBAL Rept. 694, Brooklyn, NY, May 1964; also *Prooceedings of the XI International Congress of Applied Mechanics*, edited by H. Görtler, Springer-Verlag, Berlin, 1966, pp. 299–305.

[13] Almroth, B. O., "Collapse Analysis for Elliptical Cones," *AIAA Journal*, Vol. 9, No. 1, 1971, pp. 32–37. doi:10.2514/3.6121

[14] Chen, Y. N., Feinstein, G., and Kempner, J., "Buckling of Clamped Oval Cylindrical Shells Under Axial Compresion," *AIAA Journal*, Vol. 9, No. 9, 1971, pp. 1733–1738. doi:10.2514/3.6423

[15] Feinstein, G., Erickson, B., and Kempner, J., "Stability of Oval Cylindrical Shells," *Experimental Mechanics*, Vol. 11, No. 11, 1971, pp. 514–520. doi:10.1007/BF02327691

[16] Soldados, K. P., and Tzivanidis, G. J., "Buckling and Vibrations of Cross-Ply Laminated Non-Circular Cylindrical Shells," *Journal of Sound and Vibration*, Vol. 82, No. 3, 1982, pp. 425–434. doi:10.1016/S0022-460X(82)80023-0

[17] Sun, G., "Buckling and Initial Post-Buckling Behavior of Laminated Oval Cylindrical Shells Under Axial Compression," *Journal of Applied Mechanics*, Vol. 58, No. 3, 1991, pp. 848–851. doi:10.1115/1.2897275

[18] Sheinman, I., and Firer, M., "Buckling Analysis of Laminated Cylindrical Shell with Arbitrary Cross-Section," *AIAA Journal*, Vol. 32, No. 3, 1994, pp. 648–654. doi:10.2514/3.12033

[19] Firer, M., and Sheinman, I., "Nonlinear Analysis of Laminated Noncircular Cylindrical Shells," *International Journal of Solids and Structures*, Vol. 32, No. 10, 1995, pp. 1405–1416. doi:10.1016/0020-7683(94)00191-X

[20] Soldados, K. P., "Nonlinear Analysis of Transverse Shear Deformable Laminated Composite Cylindrical Shells Part I: Derivation of Governing Equations," *Journal of Pressure Vessel Technology*, Vol. 114, No. 1, 1992, pp. 105–109. doi:10.1115/1.2928999

[21] Soldados, K. P., "Nonlinear Analysis of Transverse Shear Deformable Laminated Composite Cylindrical Shells Part II: Buckling of Axially Compressed Cross-Ply Circular and Oval Cylinders," *Journal of Pressure Vessel Technology*, Vol. 114, No. 1, 1992, pp. 110–114. doi:10.1115/1.2929000

[22] Sambandam, C. T., Patel, B. P., Gupta, S. S., Munot, C. S., and Ganapathi, M., "Buckling Characteristics of Cross-Ply Elliptical Cylinders Under Axial Compression," *Composite Structures*, Vol. 62, No. 1, 2003, pp. 7–17. doi:10.1016/S0263-8223(03)00079-5

[23] Patel, B. P., Munot, C. S., Gupta, S. S., Sambandam, C. T., and Ganapati, M., "Application of Higher-Order Finite Element for Elastic Stability Analysis of Laminated Cross-Ply Oval Cylindrical Shells," *Finite Elements in Analysis and Design*, Vol. 40, Nos. 9–10, 2004, pp. 1083–1104. doi:10.1016/j.finel.2003.06.001

[24] Haynie, W. T., and Hyer, M. W., "Torsional Loading of Noncircular Composite Cylinders," *49th AIAA/ASME/ASCE/AHS/ASC Structures, Structural Dynamics, and Materials Conference*, AIAA Paper 2008-2171, 2008.

[25] Gajewski, A., and Zyczkowski, M., *Optimal Structure Design Under Stability Constraints*, Kluwer, Dordrecht, The Netherlands, 1988. ISBN 90-247-3612-9

[26] ABAQUS Ver. 6.6, Hibbit, Karlsson, & Sorensen, Inc., Pawtucket, RI.


G. Schoeppner
*Associate Editor*